RSC Advances

PAPER

View Article Online
View Journal | View Issue

Cite this: *RSC Adv.*, 2020, **10**, 36201

Potent *in vivo* antimalarial activity of water-soluble artemisinin nano-preparations†

Praveesh Valissery,‡[a] Roshni Thapa,‡[a] Jyoti Singh,‡[c] Deepak Gaur,[b] Jaydeep Bhattacharya,*[b] Agam Prasad Singh*[c] and Suman Kumar Dhar*[a]

Artemisinin is a remarkable compound whose derivatives and combinations with multiple drugs have been utilized at the forefront of malaria treatment. However, the inherent issues of the parent compound such as poor bioavailability, short serum half-life, and high first-pass metabolism partially limit further applications of this drug. In this study, we enhanced the aqueous phase solubility of artemisinin by encapsulating it in two nanocarriers based on the polymer polycaprolactone (ART-PCL) and lipid-based Large Unilamellar Vesicles (ART-LIPO) respectively. Both nanoformulations exhibit *in vitro* parasite killing activity against *Plasmodium falciparum* with the ART-LIPO performing at comparable efficacy to the control drug solubilized in ethanol. These water-soluble formulations showed potent *in vivo* antimalarial activity as well in the mouse model of malaria at equivalent doses of the parent drug. Additionally, the artemisinin-PCL nanoformulation used in combination with either pyrimethamine or chloroquine increased the survival of the *Plasmodium berghei* infected mice for more than 34 days and effectively cured the mice of the infection. We highlight the potential for polymer and liposome-based nanocarriers in improving not only the aqueous phase solubility of artemisinin but also concomitantly retaining its therapeutic efficacy *in vivo* as well.

Received 26th June 2020
Accepted 22nd September 2020

DOI: 10.1039/d0ra05597b

rsc.li/rsc-advances

1. Introduction

Malaria, a disease caused by a unicellular, apicoplast bearing parasite of the genus *Plasmodium*, continues to be a major threat to mankind. About 405 000 malaria-related deaths were recorded in 2018 alone, of which 272 000 deaths pertained to children aged under 5 years.[1] Artemisinin, an endoperoxide antimalarial, has proven to be extremely effective in managing *Plasmodium* infections.[2] This sesquiterpene lactone is a secondary metabolite of the Sweet Wormwood plant, *Artemisia annua*, and has been employed in Traditional Chinese Medicine to treat intermittent fever.[3] The purified compound, artemisinin, was found to be an extremely potent antimalarial *in vitro* and had fast-acting properties *in vivo*. However, the therapeutic efficacy of the drug is limited due to poor solubility in water leading to very low absorption after oral administration. Additionally, artemisinin has been reported to have a short half-life and high first-pass metabolism.[4] Consequently, the water-soluble semisynthetic derivatives of artemisinin, such as artemether and dihydroartemisinin, are preferred in the clinical management of the diseases.[5] Currently, artemisinin-based combination therapy (ACT) has been regarded as the first line of defense against chloroquine-resistant *Plasmodium vivax* and uncomplicated *Plasmodium falciparum* infections.[6] WHO recommends the use of artemisinin in combination with a partner drug particularly due to the high recrudescence rates following artemisinin monotherapy. This recrudescence of the parasites has been attributed to the quick elimination half-life of the drug and the inherent ability of the parasites to induce dormancy in the ring stage upon exposure to artemisinin.[7] The delayed parasite clearance following drug treatment has been associated with the emergence of artemisinin resistance.

Over the years, polymer and lipid-based nanoparticles have emerged as a promising drug delivery system and have shown improved *in vitro* and *in vivo* therapeutic efficacy of the drugs with a wide range of physicochemical properties and biological activity. The field of drug delivery research has witnessed a substantial leap after the discovery of polymer nanoparticles and liposomes. Polymeric nanoparticles possess a tightly-interlinked matrix architecture consisting of biocompatible and biodegradable polymers of natural or synthetic origin. Polycaprolactones, polyglycolide copolymers, and polylactides are some synthetic polymers whereas albumin, chitosan and alginate are some of the natural polymers.[8,9] Liposomes are spherical vesicular structures composed of lipid bilayers containing phospholipids, cholesterol, and fatty acids, that encapsulate an aqueous core.[10] Since their advent, lipid and polymer-based nanoparticles have been extensively studied in the treatment of infectious diseases including malaria for the

[a]*Special Centre for Molecular Medicine, Jawaharlal Nehru University, New Delhi, 110067, India. E-mail: skdhar@mail.jnu.ac.in; skdhar2002@yahoo.co.in*
[b]*School of Biotechnology, Jawaharlal Nehru University, New Delhi, 110067, India*
[c]*National Institute of Immunology, New Delhi, 110067, India*

† Electronic supplementary information (ESI) available. See DOI: 10.1039/d0ra05597b

‡ These authors contributed equally.

delivery of both hydrophobic and hydrophilic drugs.[11,12] These colloidal carriers have great potential not only for efficient drug delivery but also for targeting *Plasmodium*-infected erythrocytes.[13–16] Importantly, both polymer nanoparticles and liposomes have been used extensively to enhance the solubility of compounds with poor aqueous phase miscibility.[17–20] This in turn helps to improve the oral absorption and bioavailability of the drug. Liposomal formulations of artemether and artemisinin have promising active and passive targeting abilities in *in vivo* models of brain cancer.[21] A well-reported review by Roberto *et al.* that emphasizes on the importance of liposome composition due to the ability of various phospholipids to act as intercellular messengers. The inclusion of bioactive phospholipids into the lamellar scaffolds of liposomes can modulate the immune system by various mechanisms that can be further exploited for additive/synergistic biological activity.[22] Artemisinin bound albumin nanoparticles are shown to be effective in *Plasmodium berghei* infected mice.[23] Also, a study reported by Want MY and team, have shown improved therapeutic efficacy of artemisinin loaded liposomes and PLGA-based nanoparticles against experimental and murine visceral leishmaniasis respectively.[24,25] Additionally, lipid and polymer-based nano preparation of artemisinin and its derivatives have been used to target cancers and various infectious agents.[26–30]

The past decade has seen a considerable upsurge in the employment of polymer nanoparticles in clinical therapeutics. The fundamental characteristics of polymer nanoparticles such as biocompatibility, biodegradability, and prolonged plasma circulation, along with the ease of preparation, use of low-cost excipients, controlled drug release, and better stability of polymer nanoparticles make them a great candidate for cost-effective drug delivery systems.[31] On the other hand, the expensive constituents of liposomes and multi-step complex preparation increases the cost of production substantially. Moreover, the formation of lamellar structure is not thermodynamically favored making them metastable and prone to degradation during long-term storage.[32] However, conjugation of targeting ligands in liposomes have been reported to be more efficient as compared to surface functionalization of polymer nanoparticles.[33] Additionally, liposomes are reported to be good candidates for combination therapy due to its ability to accommodate both hydrophilic and hydrophobic compounds into the core and the lipid bilayers respectively. However, polymeric nanoparticles require double emulsion technique or other strategies such as pH modification, polyanion, for entrapment of water-soluble compounds.[34] Despite the challenges associated with liposome and polymer nanocarriers, these drug delivery systems have made a remarkable impact in the field of clinical therapeutics.

The life cycle of malaria parasite is complex with both mosquito and human hosts. Within the human host the parasite completes its asexual cycle *via* the liver and the erythrocytes. Since the disease manifests during the erythrocytic stage, the drugs and formulations that target this stage are of paramount importance.

In this study, we have synthesized polymer and liposome-based nanoparticles loaded with artemisinin to compare and improve its oral bioavailability and subsequent anti-malarial activity in the *in vitro* parasite culture and also in the *in vivo* animal model.

2. Materials and methods

2.1. Materials

Artemisinin (98%), poly(ε-caprolactone) (PCL) (MW 14,000), Pluronic F-127 and cholesterol were purchased from Sigma Aldrich Pvt. Ltd, India. LIPOID S PC-3, LIPOID PE 18:0/18:0-PEG 200 sodium salt were gifts from Lipoid Germany. The organic solvents used were of analytical grade and HPLC grade purity. SYBR Green I dye was purchased from ThermoFisher Scientific (S7563).

2.2. Synthesis of artemisinin loaded nanoparticles

2.2.1. Preparation of artemisinin-loaded PCL nanoparticles. Nano-precipitation method was employed for the preparation of polymer nanoparticles with modifications.[35] Artemisinin and PCL were dissolved in a water-miscible volatile organic solvent, acetone, where the aqueous phase used was 1% w/v Pluronic F127. The organic phase, containing the drug, was added in a dropwise manner to the aqueous phase using a disposable syringe. The aqueous phase was kept under constant agitation by a magnetic stirrer. The resultant suspension was left overnight under mild stirring to completely remove the volatile organic solvent.

2.2.2. Experimental design, optimization, and method validation. MINITAB 9.0 software was used for the development and optimization of ART-loaded-PCL formulation. As shown in Table 1, The quadratic response surfaces and contour plots for understanding the effects of various independent variables on the selected dependent variables were generated by using the three-level, three-factor Box–Behnken design. Polymer drug ratio (PCL:ART) (X_1), the concentration of polymer (PCL) (% w/v, X_2), and stirring time (X_3) were taken as independent variables, represented by +1, 0 and −1, which are analogous to high, medium and low levels, respectively (Table 1). The dependent variables selected were hydrodynamic radii (Y_1), zeta potential (Y_2), and entrapment efficiency (Y_3). The polynomial equation generated from the experimental design was:

$$Y = b_0 + b_1X_1 + b_2X_2 + b_3X_3 + b_{11}{X_1}^2 + b_{22}{X_2}^2 + b_{33}{X_3}^2 + b_{12}X_1X_2 + b_{13}X_1X_3 + b_{23}X_2X_3$$

where Y is the selected dependent variable, X_1 X_2, and X_3 are the independent variables, ${X_1}^2$, ${X_2}^2$ and ${X_3}^3$ are the quadratic terms; X_1X_2, X_2X_3, and X_1X_3 are the interaction terms; b_0 is the intercept whereas b_1–b_{33} are the regression coefficient based on the experimental values of Y. The observed responses were fitted into different models and the polynomial equation was validated for statistical significance using ANOVA in the MINITAB software.

2.3. Preparation of liposome nanoparticles

The artemisinin-loaded liposomes (ART-LIPO) were prepared using a conventional thin-film hydration method. The drug-

Table 1 Independent and dependent variables with the coded levels in the Box–Behnken design

		Coded levels		
Independent variables	Symbols	−1	0	+1
Polymer: drug	X_1	1	2	3
Polymer concentration (w/v%)	X_2	0.1	0.2	0.3
Stirring time (h)	X_3	1	2	3
Dependent variables	Symbols	Constraints		
Hydrodynamic radii	Y_1	Optimum (50–150 nm)		
Zeta potential	Y_2	±25		
% entrapment efficiency	Y_3	Maximum		

loaded liposomes were synthesized using LIPOID S PC-3 and LIPOID PE-PEG, which are hydrogenated soy phospholipid and the sodium salt of PEGylated phosphoethanolamine respectively. Additionally, cholesterol was incorporated into the preparation to impart membrane fluidity and permeability of the drug into the liposomes.[36] In a round-bottom flask, the drug and the lipophilic components, phospholipids and cholesterol, were solubilized in chloroform. The organic solvent, chloroform, was completely evaporated at 45 °C using Rotavapor Film Evaporator under low pressure. After complete evaporation of the solvent, the resulting thin film was rehydrated using PBS containing 0.85% NaCl. To produce Large Unilamellar Vesicles (LUVs), the resultant multilamellar liposomes were bath-sonicated for 30 min followed by 10 cycles of manual extrusion.

2.4. Characterization of artemisinin-loaded nanoparticles

2.4.1. Particle size and size distribution. The Dynamic Light Scattering (DLS) technique using the Zetasizer Nano ZS (Malvern) was employed to determine the size distribution of the ART-PCL and ART-LIPO nanoparticles. The samples were diluted using Milli-Q water to a concentration of approximately 2.5×10^{21} particles per ml for PCL nanoparticles and 2.8×10^{20} particles per ml for liposomes. The number of particles was calculated using the following equation reported by Shang J. and Gao X.[37]

$$c = N/N_A V$$

where c is the molar concentration; N is the total number of particles in the colloidal suspension; N_A is the Avogadro constant and V is the total volume of colloidal suspension.

The hydrodynamic radii of diluted suspensions of nanoparticles, which represents the particle size of the generated nanocarriers, were measured at 90° detection angle at room temperature (25 ± 2 °C). The DLS measurements reported are the mean of multiple runs ($n = 3$). The Polydispersity Index (PDI) of the particles was also measured.

2.4.2. Zeta potential. Zetasizer Nano ZS (Malvern) was used for the measurement of zeta potential. Capillary electrophoresis cells were used to measure the zeta potential of the nanoparticles, diluted using deionized water. The resultant measurements were the average of triplicate runs.

2.5. Surface morphology and shape

The surface morphology of the optimized ART-PCL nanoparticles and ART-LIPO was analyzed using Scanning Electron Microscope (Zeiss EVO40). The concentrated nanoparticle population was drop cast on a conducting surface and vacuum dried, followed by gold coating. Transmission Electron Microscopy using (TEM-JEOL-2100F) images of ART-LIPO was taken and analyzed to confirm the shape of the vesicles that were generated. The concentrated suspension was placed onto 300-mesh copper-coated carbon grids. To enhance the electron density of the samples, the samples were negatively stained using phosphotungstic acid.

2.6. Entrapment efficiency

The entrapment efficiency of the ART-PCL and ART-LIPO was calculated as reported earlier with some modifications.[38] The nanoparticle suspensions were centrifuged at 13 000 rpm for 30 minutes. The supernatant was isolated and analyzed using a UV-vis spectrophotometer to determine the concentration of un-entrapped drug in the supernatant.

The percentage of entrapment efficiency was calculated using the following formula:

$$\%\ \text{entrapment efficiency} = \frac{(\text{total ART added} - \text{free ART in the supernatant})}{\text{the total amount of ART added}} \times 100$$

2.7. *Plasmodium falciparum* culture and *in vitro* assay growth inhibition assay

2.7.1. Plasmodium falciparum culture. The erythrocytic, asexual stage of the *Plasmodium falciparum* 3D7 strain of parasites were cultured in (O+) human red blood cells. They were maintained in RPMI 1640 medium supplemented with 0.5% Albumax-II, 0.2% $NaHCO_3$, 10 μg ml^{-1} of gentamycin sulfate, and 27 mg per liter of hypoxanthine. The culture is kept in airtight culture flasks gassed with a mixture of 90% nitrogen, 5% CO_2, and 5% O_2 and maintained at 37 °C. Parasites were double synchronized before any *in vitro* experiments. This was done using the standard sorbitol synchronization method.[39] Asynchronous parasites were incubated for 5 minutes at 37 °C with 5% sorbitol. The culture was centrifuged to remove the sorbitol. This was followed by two washes of incomplete RPMI medium (containing no Albumax-II) and one final wash with the complete RPMI medium. Thin smears of culture on glass slides were prepared each day and stained with Giemsa after fixing with methanol. These slides were observed under a simple brightfield microscope (Nikon) for monitoring parasitemia and the stage of the parasites.

2.7.2. *In vitro Plasmodium* growth inhibition. Double synchronized ring-stage parasites were aliquoted to a 96-well plate (NUNC, FluroLumi) at 2% hematocrit and 1%

parasitemia. The nanoformulations were solubilized in deionized and demineralized water. Stock solutions of 1 mg ml^{-1} were prepared and the aliquots were made immediately before use, after 30 seconds of vigorous vertexing. Artemisinin positive controls were prepared as 1 mg ml^{-1} stocks in ethanol. After 48 h of incubation with varying concentrations of the drug formulation, the plates were ready for quantitation of parasitemia. Initially, the antimalarial activity of various formulations was quantitated manually. Thin smears of the treated and untreated parasite culture were made and stained by Giemsa staining. By direct microscopy, the stained parasites were counted against empty RBC in various fields of view to afford the mean parasitemia of the culture. For precise quantitative measurements, an adaptation of the SYBR Green I assay was employed.[40] The treated 96-well culture plates were freeze-thawed to rupture the RBC. The SYBR Green I lysis buffer was prepared; its composition includes Tris 200 mM (pH 7.5), EDTA (5 mM), saponin (0.008% w/v), and Triton X-100 (0.08%, w/v) with 0.1 μl ml^{-1} of SYBR Green I dye. 100 μl of the buffer was added to each well and the plates were incubated for 2 h in complete darkness. A 96-well fluorescence plate reader (Thermo VARIO SKAN), was used to read the plates. The excitation wavelength was taken as 497 nm and emission wavelength was 520 nm. The readings were normalized and plotted against a log scale of the drug concentration. The dose–response plots were generated and IC_{50} values were calculated using GraphPad Prism 6 (San Diego, CA) software. The fluorescence data were fitted in a nonlinear regression model (sigmoidal dose–response/variable slope) to yield the IC_{50} value.

2.8. Animals and *in vivo* inhibition assay

2.8.1. Animals and parasite. Male/female (6–8 weeks) C57BL/6 or BALB/C mice were used in the experiments. All animal-related work was performed following the NII Institutional Ethics Committee (IAEC) approved protocols. IAEC approval for this work is detailed in approval number 448/17. Animals were housed at room temperature (~25 °C) and 12:12 light/dark cycle. Mice were given food and water ad libitum. Internationally accepted laboratory norms for animal use were followed in all experiments. Mice were injected with xylazine/ketamine intraperitoneally for short-term anesthesia. At the end of each experiment, anesthetized mice were humanely sacrificed by cervical dislocation. Erythrocytic stage parasites were maintained by weekly serial passage of parasite containing blood into the non-infected mice.

2.8.2. Parasite inoculation. Donor mice (C57BL/6 or Balb/C) with high parasitemia (5–20%) and infected with *P. berghei* were used. Blood from donor mice was collected by opening the thoracic region. Anticoagulants were mixed with blood at the time of collection to avoid clotting. Sterile PBS was used to dilute the blood where necessary.

2.8.3. *In vivo* suppressive test. Four-day parasite suppression test was performed to know the schizonticidal activity of the formulations. This was done as per a method described by Peters *et al.* with some modifications.[41] The mice were arbitrarily divided into groups of 5 each. The mice were injected with parasites on day 1 and the drug treatments commenced after 24 hours. The treatment continued for the next 4 days. Mice survival was observed daily up to 28 days of post-treatment initiation. The mean survival time was calculated for each group. Giemsa-stained thin blood smears were prepared, and the percentage of parasite growth suppression (PGS) was estimated by the formula: $[A - B/A] \times 100$, where A is the average parasitemia of control (negative) group and B, represents the parasitemia of the experimental group.

2.8.4. *In vivo* antimalarial activity of artemisinin nanoformulations and drug combinations. Mice infected with *P. berghei*-NK65 (5–20% parasitemia) were used as donors. Experimental mice (C57BL/6) were randomly divided into 6 groups, each group having 4 mice. The mice were injected intraperitoneally (I.P.) with 1.0×10^7 parasitized erythrocytes. Treatment started 24 hours post parasite inoculation on day one. Treatments continued (beginning day 1 to day 5) for 5 days. Group 1 was a control group where the animal did not receive any drug. Group 2 was artemisinin nano; where animals received formulation at a dose of 50 mg per kg per day in 200 μL. Group 3 was chloroquine only where animals received intraperitoneally dose of 20 mg per kg per day in 200 μL on 4th and 5th days. Group 4 was pyrimethamine alone, animals received two doses on 4th and 5th days @10 mg per kg per day in 200 μL. Group 5 was artemisinin nano along with chloroquine; animals received artemisinin nanoformulation on the 1^{st} 2^{nd} and 3^{rd} day and chloroquine I.P @ 20 mg per kg per day in 200 μL on the last two days. Group 6 was artemisinin nano along with pyrimethamine, animals received artemisinin nanoformulation on the first three days and pyrimethamine I.P @ 10 mg per kg per day in 200 μL on the last two days. For establishing significance between groups, mice that died of natural causes with low parasite loads were removed from analysis as was the case with a mouse in the artemisinin PCL and pyrimethamine combination treated group. To calculate parasitemia, Giemsa-stained blood smears were counted using a brightfield microscope. Smears were prepared from the tail of each animal. Percentage inhibition of the parasite was calculated using the formula mentioned in method Section 2.8.3. Mean survival time (MST) was determined for each group over 28 days.

2.9. Statistical analysis

Statistical analysis was conducted using Graphpad Prism (version 8.0.1.). For *in vivo* studies, one-way ANOVA followed by Sidak's multiple comparisons test was used to assess the

Table 2 Physicochemical properties of artemisinin loaded PCL nanoparticles and liposomes

Drug-loaded nanoformulations	ART-PCL	ART-LIPO
Hydrodynamic radii (rpm)	123 ± 6.6	147 ± 4.7
Polydispersity index (PI)	0.181 ± 0.032	0.2 ± 0.021
Zeta potential (mV)	−13.2 ± 3.35	−16 ± 1.28
Entrapment efficiency (%)	67.8 ± 2.17	81.68 ± 3.72

significance of the results. Statistical significance is represented as $*p < 0.05$, $**p < 0.01$, $***p < 0.001$.

3. Results

3.1. Formulation, development, and optimization of artemisinin loaded PCL and liposome nanoparticles

The 3-factors 3-level Box-Behnken design generated 15 sets of experiments. They were further assessed for resultant dependent variables namely, hydrodynamic radii, zeta potential, polydispersity index, and entrapment efficiency (ESI Table 1†). Based on the polynomial equation for each dependent variable, the influence of independent variables was studied. The hydrodynamic radii of the PCL nanoparticles were found to increase with increasing polymer concentrations. This may be a result of the rise in the viscosity of the organic phase which may lead to the generation of bigger nano-droplets. The increase in viscosity of the organic phase has been shown to increase the resistance of drug diffusion into the aqueous phase.[38,42] This helps to improve the entrapment efficiency of the formulation. The increase in stirring time from 1 hour to 3 hours did not exhibit a significant effect on the particle size. The

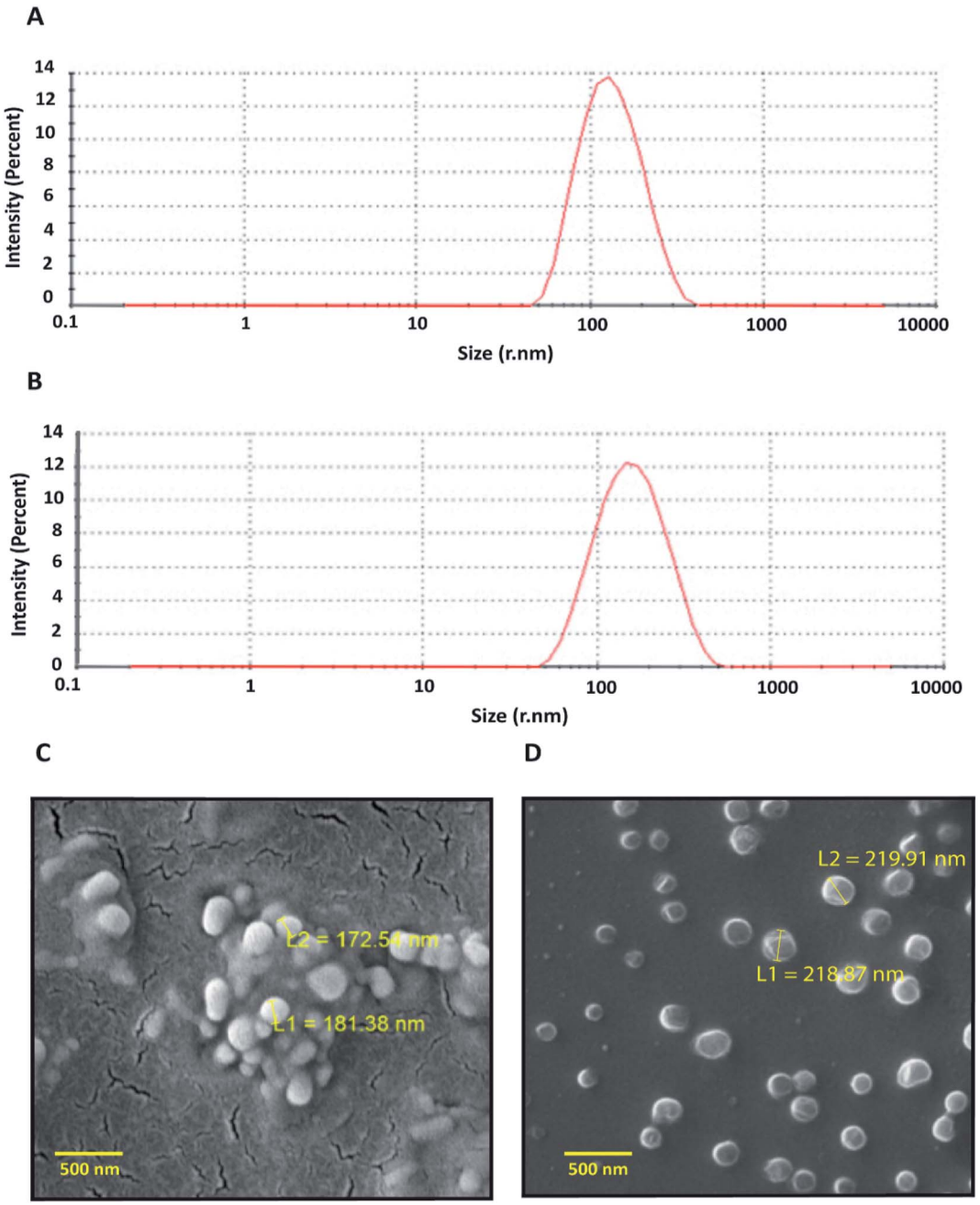

Fig. 1 Characterization of artemisinin loaded nanoparticles. (A) Particle size distribution of ART-PCL. (B) Particle size distribution of ART-LIPO particles. The DLS plots were drawn from the mean of results obtained from three technical replicate runs. (C) SEM image of ART-PCL. (D) SEM image of ART-LIPO. L1 and L2 are diameters of individual particle.

hydrodynamic radii of ART-PCL varied from 94.86 to 126.5 nm at different synthesis conditions (ESI Table 1†).

Different sets of experimental runs produced ART-PCL nanoparticles with zeta potential ranging from −13 to −23.7 mV. Based on the results obtained from ESI Table 1,† the optimized formulation with a polymer–drug ratio of 3, a polymer concentration of 0.3%, and a stirring time of 1 hour was chosen for further studies. The resultant optimized formulation was found to have the hydrodynamic radii of 123 ± 6.6 nm, zeta potential −13.2 mV, and 67.8% drug entrapment efficiency (Table 2).

As per the statistical data generated, the polymer concentration was found to have the most significant impact on zeta potential; whereas stirring time and polymer–drug ratio showed minor influences. The percentage of entrapment efficiency (EE) of the formulations was found to vary between 36–71%. The ANOVA analysis of results showed that the independent variables like polymer concentration and polymer–drug ratio had a significant role in controlling the entrapment efficiency. Higher polymer concentration led to an increase in entrapment efficiency whereas the higher polymer–drug ratio showed a decrease in drug entrapment. Based on the above results, the optimized formulation having the hydrodynamic radii of 123 ± 6.6 nm, zeta potential −13.2 mV, and entrapment efficiency of 67.8%, were used for the biological studies. The particle size distribution and scanning electron microscopic images of the optimized formulation indicates that the particles were monodisperse and spherical (Fig. 1 A and B).

ART-LIPO nanoparticles were synthesized using conventional thin-film hydration followed by bath sonication and manual extrusion. To increase the *in vivo* plasma circulation time of liposomes, stealth liposomes were formulated by including PEGylated phospholipid into the formulation. The drug-loaded liposomes were highly monodisperse having the hydrodynamic radii of 143 ± 4.7 nm with the polydispersity index of 0.20 when measured using DLS (Fig. 1C). ART-LIPO showed high drug entrapment efficiency of up to 81.68% and high stability with the zeta potential of −16 mV. They were also found to be spherical when viewed by scanning electron microscopy (Fig. 1D).

3.2. Artemisinin nano-formulations show *in vitro* antimalarial activity

The physical entrapment efficiency of the formulations was calculated before conducting any *in vitro* experiments. Based on the entrapment efficiency, the equivalent concentration of each nanoformulation was calculated concerning the free drug. Drug dilutions were made accordingly such that equimolar amounts of artemisinin were present in the nanoformulation and the positive control. The nano preparation was diluted in water and the *in vitro* antimalarial activity was examined (Fig. 2).

Both the nano preparation retained their antimalarial activity with ART-PCL showing 5.6 times higher IC_{50} compared to the ethanol solubilized compound. ART-LIPO performed as good as the native compound. The IC_{90} values of ART-PCL and ART-LIPO were 108.9 ± 7.6 nM and 33.27 ± 4.76 nM respectively. The IC_{90} of ART-LIPO is much closer than ART-PCL to artemisinin Native (IC_{90} = 21.27 ± 1.28 nM), but it is 1.5 times higher. Given that their IC_{50} values are similar, the slightly higher IC_{90} of ART-LIPO might suggest a slight decrease in drug release with increasing concentration of the formulation *in vitro*.

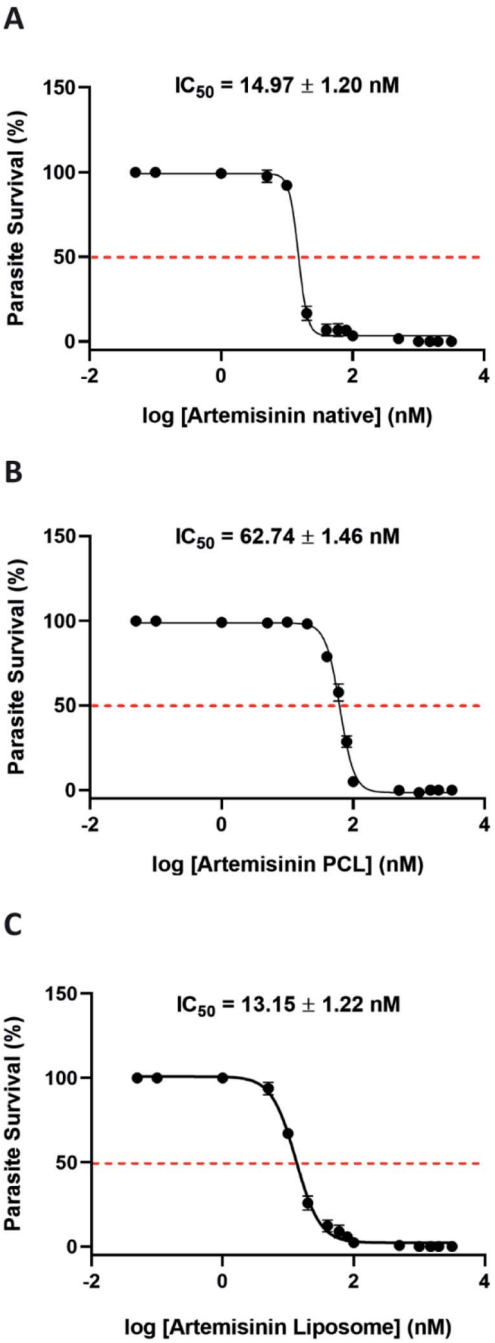

Fig. 2 Artemisinin (ART) based nano formulations have potent antimalarial activity. Dose response curves of (A) artemisinin native, (B) artemisinin PCL (C) artemisinin liposomes were generated by incubating synchronized ring stage parasites with increasing concentrations of the drug formulation for a period of 48 h and the parasitemia was estimated by SYBR green I assay.

The vehicle controls containing the nanocarriers alone did not show any significant antimalarial activity (ESI Fig. 1 and 2†). It is important to note that artemisinin alone is not soluble in water and does not retain any antimalarial activity in aqueous solvents (ESI Fig. 3†).

3.3. Potent *in vivo* anti-malarial activity of artemisinin nano-formulations

The PCL and liposome encapsulated artemisinin nano formulations showed potent antimalarial activity against the rodent-infecting *Plasmodium berghei*; the mouse model of malaria (Fig. 3). The drug treatment was given for five days. As seen on day 9 post-infection, both nanoformulations performed similarly to the ethanol solubilized artemisinin treated groups. ART-PCL and ART-LIPO treated groups showed an 85.5% and 85.14% reduction in parasitemia compared to the untreated control group, respectively.

The PCL vehicle control-treated groups showed a growth rate similar to the untreated control group. On day 9, the difference between the PCL vehicle control-treated group and the untreated control group was not statistically significant. However, the liposome vehicle-treated group showed a statistically significant reduction in parasitemia compared to the untreated control group at day 9 post-infection (p-value = 0.0242). We also used artesunate (water) as a positive control that showed parasitemia beyond the detection limit, *i.e.* 9th-day post-infection. These results suggest that the water-soluble nanoformulation of artemisinin is as efficient as artemisinin in ethanol.

3.4. Artemisinin PCL nanoformulations can be used in combination with partner drugs without any adverse complications *in vivo*

As per the WHO directives, artemisinin is rarely given as a single drug for malaria therapy. To avoid the emergence of resistance, artemisinin is often given in combination with a known antimalarial with a unique mechanism of action and long serum half-life.[43] To evaluate the efficacy of ART nanoformulations along with other malaria drugs, *Plasmodium berghei* infected mice were treated with the PCL encapsulated artemisinin nanoformulation in combination with chloroquine and pyrimethamine. At day 14 post-infection, there was a statistically significant reduction in parasitemia in the artemisinin PCL and chloroquine treated groups compared to the artemisinin PCL only treated group (Fig. 4A and B). Additionally, the groups treated with artemisinin and a partner drug survived significantly longer than the drug mono-treated groups (Fig. 4C). These results suggest that combining artemisinin PCL with a partner drug did not have any adverse effects on the animal and additionally improved its survival.

4. Discussion

Here, we have shown that artemisinin, a powerful water-insoluble antimalarial, can be made soluble using polymer and liposome-based nanocarriers without compromising its antimalarial activity.

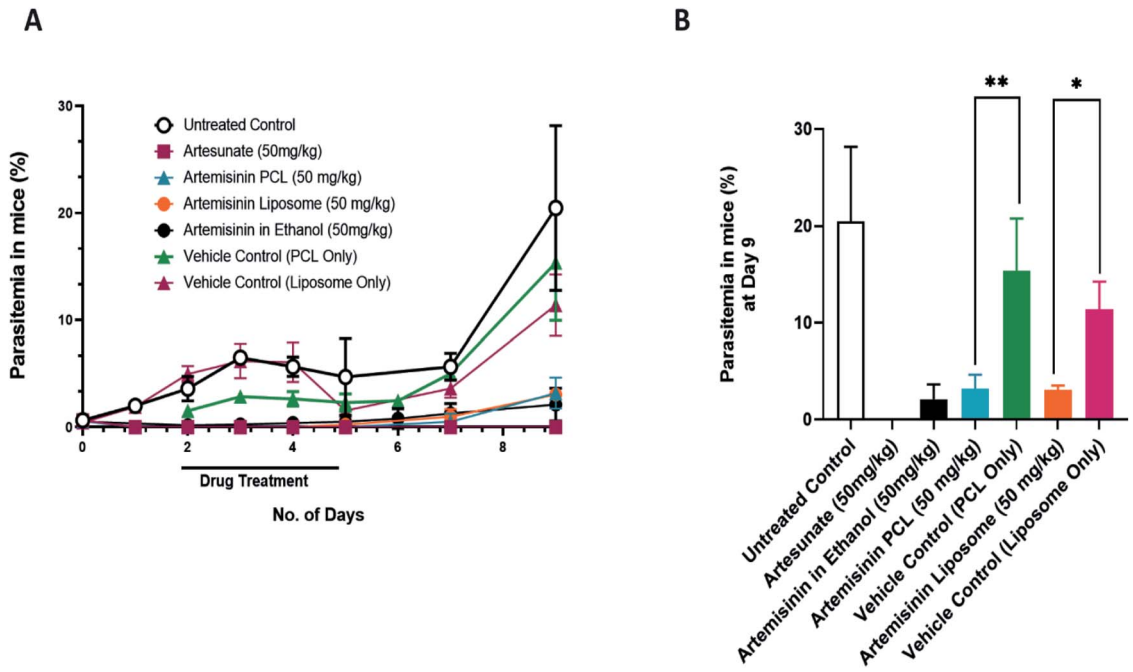

Fig. 3 *In vivo* antimalarial activity of artemisinin nano-formulations. Drug treatment was given for a period of 5 days. Artesunate (50 mg kg^{-1}) was used as a positive control. (A) Shows mean parasitemia at various days post infection upon treatment with artemisinin PCL and artemisinin liposome nano-formulations. (B) Represents average parasitemia at day 9 post infection upon treatment with ART-PCL and ART-LIPO. Values are plotted as means ± the standard error of the mean, SEM (n = 4 mice/group). Statistical significance was established after performing one-way ANOVA followed by Sidak's multiple comparisons test where *p < 0.05, **p < 0.01, ***p < 0.001.

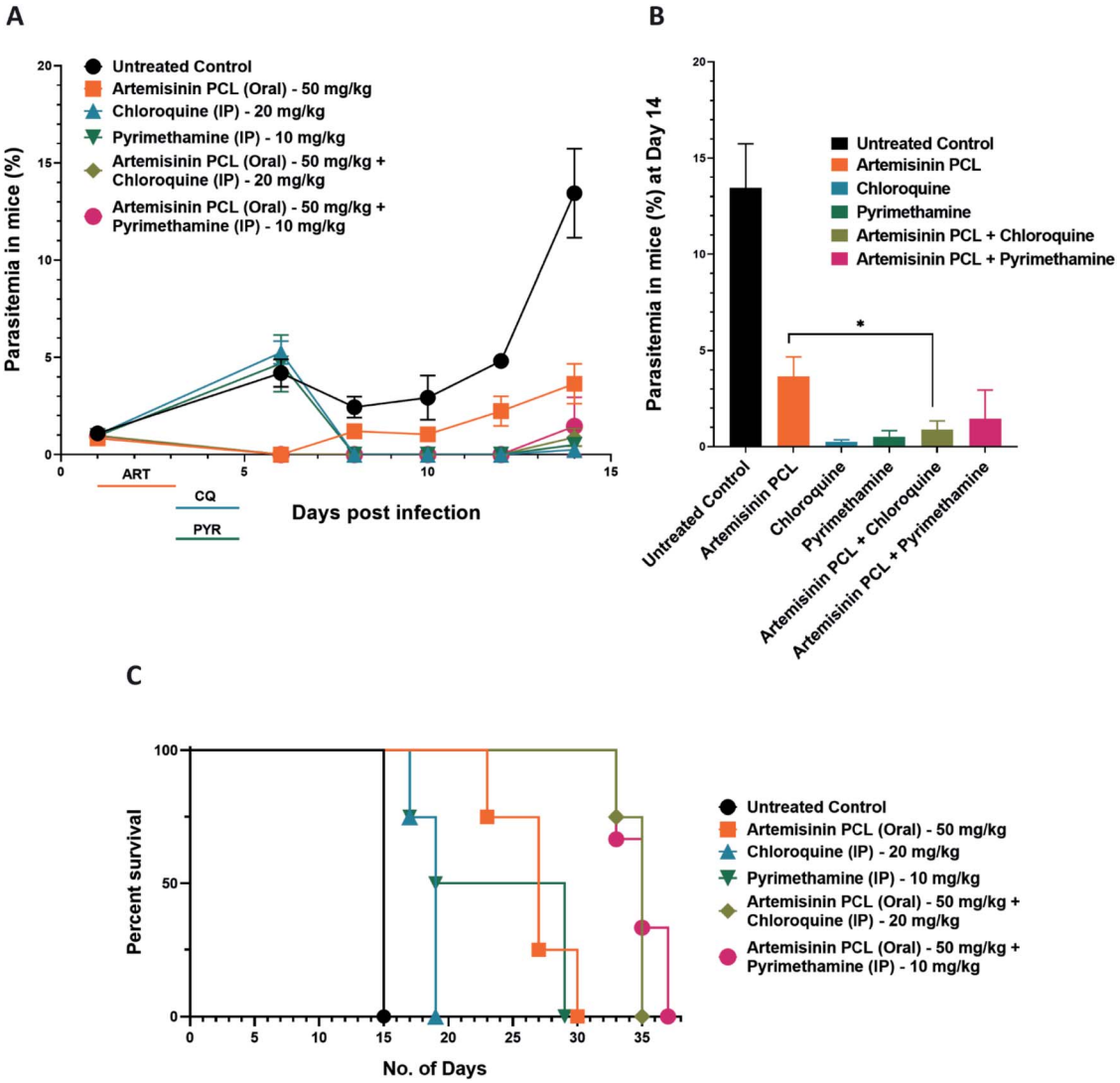

Fig. 4 *In vivo* antimalarial activity of artemisinin PCL nano-formulation given in combination with chloroquine or pyrimethamine. Artemisinin (50 mg kg^{-1}) was given for 3 days *via* oral route. Chloroquine (20 mg kg^{-1}) and pyrimethamine (10 mg kg^{-1}) were given for 2 days *via* intraperitoneal injections. (A) Shows mean parasitemia at various days post infection upon treatment with artemisinin PCL nano-formulation and the partner drugs. (B) Represents average parasitemia at day 14 post infection. (C) Kaplan Meier survival curve showing the survival of the combination and monodrug treated mice against an untreated control for a period of 28 days. Values are plotted as means ± the standard error of the mean, SEM ($n = 4$ mice/group). Statistical significance was established after performing one-way ANOVA followed by Sidak's multiple comparisons test where *$p < 0.05$, **$p < 0.01$, ***$p < 0.001$.

Both, the drug-loaded PCL and liposome based nanoparticles have the desired size in the range of 120–150 nm and possess optimal encapsulation efficiencies of 67.8% and 81.68% respectively. Based on the *in vitro* tests, it was evident that the ART-LIPO formulation was successful in completely retaining the anti-malarial activity of the drug while encouraging the aqueous phase solubility. However, when it came to the *in vivo* performance of the formulation, we found that the LIPO nanocarrier alone showed a statistically significant reduction in parasite load in the absence of the drug. This suggests that the unloaded liposome vehicle might possess inherent anti-plasmodial activity. This may be attributed to the tendency of the chemical constituents of the liposome to trigger the innate immune response of the host, particularly the complement cascade[44–46] and macrophage-mediated clearance mechanisms.[47] This host response might unwittingly aid in the clearance of parasitized RBC within the animal.[48] Some liposome-based formulations like Doxil, Ambisome, Visudyne, and DaunoXome have been shown to stimulate C activation-related pseudoallergy (CARPA) in the blood by reacting with complement proteins.[49–52] Such liposome-mediated immune responses have been leveraged in cancer therapy due to the stimulation of anti-tumor immune effectors.[53,54] While the background antimalarial activity of the LIPO nanocarrier alone may be beneficial, it prevents us from accurately estimating the efficacy of the drug within the formulation. Therefore, we focused on the more definite ART-PCL for the drug combination studies. The antiplasmodial property of the liposome carrier is

an intriguing phenomenon. We hope to further expand on this observation by testing with similar liposome building lipids in the future.

Though the *in vitro* IC_{50} of the ART-PCL formulation was 5.6 times that of the parent drug, the formulation behaved similarly to artemisinin in ethanol and performed competently *in vivo*. Though the formulation did not enhance the antimalarial activity of the drug, the compound has become soluble in water. We hypothesized that by improving the drug's aqueous phase solubility, we can enhance the oral bioavailability and increase the elimination half-life of the drug. However, this is not represented in the *in vivo* antimalarial effect. The interaction of the nanocarrier shell with the various proteins and factors in the blood plays a major role in determining the clearance and uptake of the formulation and therefore greatly impacts its delivery and distribution to the drug target.[55] Consequently, the physical makeup of the nanocarrier is the most decisive factor in ensuring its *in vivo* efficacy. The absence of such intricate interactions *in vitro* demonstrates the stark difference in the efficacy of the ART-PCL formulation between the *in vitro* and *in vivo* studies. Nonetheless, we find that the improved solubility allows for a higher dosing regimen to be implemented. This works in our favor as it has been seen in both animal and human studies that long-term persistence of the drug, rather than a short-term spike in serum concentration of artemisinin can cause toxicity to the host.[56]

In this context we have to consider the release kinetics of the nanoformulations. There are several reports of sustained drug release varying from 72 hours to 100 hours using similar polymer nanoparticles that were used in our study. As reported by Rutina Li *et al.*, a burst release profile was seen in drugs entrapped in the PEG-PCL nanoparticles. Up to 50% of burst release was observed in under 10 hours followed by a sustained release for another 4 days.[57] Another study conducted by Yang *et al.* compares the release profile of hydrophobic (Cisplatin) and hydrophilic (Gemcitabine) drugs entrapped in PCL nanoparticles. The PCL nanoparticles with the mean diameter of 160 $\pm$ 5 nm showed a more sustained release of the hydrophobic molecule as compared to the hydrophilic drug.[58] On the other hand, the drug release patterns of the multilamellar vesicular liposomes were found to be less sustained as compared to polymer nanoparticles. Reports show that almost 80% of the drug was released in less than 10 hours.[59–61] Interestingly, initial burst release is observed in both polymer and lipid nanoparticles but comparatively more in the case of polymer nanoparticles. This could be due to the desorption of some of the adsorbed drug on the surface of polymer nanoparticles. The release kinetics of polymer nanoparticles is mainly driven by diffusion of the drug and bioerosion of the polymer in the serum whereas drug release from the liposomes is mainly due to diffusion and enzymatic degradation of the lipid components.[62]

Another aspect of the ART-PCL formulation is its ability to be used in combination with a partner drug without any negative effects. Both partner drugs tested, chloroquine, and pyrimethamine given individually in conjugation with ART-PCL improved the survival of the animal drastically. This may be attributed to the usage of partner compounds with unique mechanisms of action. Chloroquine for instance targets the heme polymerization to hemozoin in the parasite.[63] This is a crucial detoxification process, that is essential in preventing the buildup of toxic free heme that is generated during hemoglobin breakdown. Pyrimethamine targets the dihydrofolate reductase protein, an indispensable component of the DNA/RNA precursor synthesis machinery.[64] When these compounds are used in conjunction with artemisinin, a drug that is shown to have multiple molecular targets within the parasite, their potency is further compounded by the inclusion of newer molecular targets and therefore exhibit an additive effect.[65,66]

5. Conclusions

Though the nanoformulation did not enhance the antimalarial activity of artemisinin, we find that improving its solubility is a step in the right direction. Next, we hope to utilize the versatility of these nanocarriers by chemically conjugating antibodies specific to protein epitopes expressed on the *Plasmodium*-infected RBC surface. This may enhance the efficacy of the drug while minimizing the undesirable off-target effects. In addition to this, we hope to explore the potential in encapsulating multiple drugs in a single nanocarrier species to allow for a more efficient means of delivering immiscible drug combinations *in vivo*.

Conflicts of interest

There are no conflicts to declare.

Acknowledgements

PV acknowledges the University Grant Commission, India for fellowship. RT and JS acknowledge the Department of Biotechnology (DBT), Govt of India for fellowships. SKD, APS, DG, and JB acknowledge DBT, India for funding (BT/PR21569/NNT/28/1234/2017). SKD acknowledges the Department of Science and Technology, SERB, Govt of India (DPRP) for financial assistance. The authors acknowledge AIRF SEM Facility, JNU for their technical support in electron microscopy imaging and Seemalata Uchoi for providing assistance with certain experiments.

Notes and references

1 WHO, *World Malaria Report 2019*, https://apps.who.int/iris/rest/bitstreams/1262394/retrieve, Page No. 10 and 11, accessed May 17, 2020.
2 N. J. White, *Antimicrob. Agents Chemother.*, 1997, **41**, 1413–1422.
3 W. Fu, *Chinese Medicine and Culture*, 2018, **1**, 18–20.
4 I. Charlie-Silva, L. F. Fraceto and N. F. S. de Melo, *Artif. Cells, Nanomed., Biotechnol.*, 2018, **46**, S611–s620.
5 C. A. Morris, S. Duparc, I. Borghini-Fuhrer, D. Jung, C.-S. Shin and L. Fleckenstein, *Malar. J.*, 2011, **10**, 263.

6 L. Cui and X.-z. Su, *Expert Rev. Anti-Infect. Ther.*, 2009, **7**, 999–1013.
7 M. Ouji, J.-M. Augereau, L. Paloque and F. Benoit-Vical, *Parasite*, 2018, **25**, 24.
8 E. Calzoni, A. Cesaretti, A. Polchi, A. Di Michele, B. Tancini and C. Emiliani, *J. Funct. Biomater.*, 2019, **10**, 4.
9 J. P. Rao and K. E. Geckeler, *Prog. Polym. Sci.*, 2011, **36**, 887–913.
10 L. Sercombe, T. Veerati, F. Moheimani, S. Y. Wu, A. K. Sood and S. Hua, *Front. Pharmacol.*, 2015, **6**, 286.
11 A. A. Date, M. D. Joshi and V. B. Patravale, *Adv. Drug Delivery Rev.*, 2007, **59**, 505–521.
12 N. Puttappa, R. S. Kumar, G. Kuppusamy and A. Radhakrishnan, *Acta Trop.*, 2019, **195**, 103–114.
13 E. Moles, P. Urbán, M. B. Jiménez-Díaz, S. Viera-Morilla, I. Angulo-Barturen, M. A. Busquets and X. Fernàndez-Busquets, *J. Controlled Release*, 2015, **210**, 217–229.
14 N. Jawahar, U. K. Baruah and V. Singh, *J. Pharm. Sci. Res.*, 2019, **11**, 33–40.
15 A. A. Sidhaye, K. C. Bhuran, S. Zambare, M. Abubaker, N. Nirmalan and K. K. Singh, *Nanomedicine*, 2016, **11**, 2809–2828.
16 M. Marwah, P. Narain Srivastava, S. Mishra and M. Nagarsenker, *Int. J. Pharm.*, 2020, **587**, 119710.
17 Y. Chen, Y. Lu, J. Chen, J. Lai, J. Sun, F. Hu and W. Wu, *Int. J. Pharm.*, 2009, **376**, 153–160.
18 M. Rai, A. P. Ingle, R. Pandit, P. Paralikar, N. Anasane and C. A. D. Santos, *Expert Rev. Anti-Infect. Ther.*, 2020, **18**, 367–379.
19 A. Bhakay, M. Rahman, R. N. Dave and E. Bilgili, *Pharmaceutics*, 2018, **10**, 86.
20 M. K. Lee, *Pharmaceutics*, 2020, **12**, 264.
21 X. Y. Li, Y. Zhao, M. G. Sun, J. F. Shi, R. J. Ju, C. X. Zhang, X. T. Li, W. Y. Zhao, L. M. Mu, F. Zeng, J. N. Lou and W. L. Lu, *Biomaterials*, 2014, **35**, 5591–5604.
22 R. Nisini, N. Poerio, S. Mariotti, F. De Santis and M. Fraziano, *Front. Immunol.*, 2018, **9**, 155.
23 N. Ibrahim, H. Ibrahim, A. M. Sabater, D. Mazier, A. Valentin and F. Nepveu, *Int. J. Pharm.*, 2015, **495**, 671–679.
24 M. Y. Want, M. Islamuddin, G. Chouhan, H. A. Ozbak, H. A. Hemeg, A. K. Dasgupta, A. P. Chattopadhyay and F. Afrin, *Colloids Surf., B*, 2015, **130**, 215–221.
25 M. Y. Want, M. Islammudin, G. Chouhan, H. A. Ozbak, H. A. Hemeg, A. P. Chattopadhyay and F. Afrin, *Int. J. Nanomed.*, 2017, **12**, 2189–2204.
26 M. Jabbarzadegan, H. Rajayi, M. A. Mofazzal Jahromi, H. Yeganeh, M. Yousefi, Z. Muhammad Hassan and J. Majidi, *Artif. Cells, Nanomed., Biotechnol.*, 2017, **45**, 808–816.
27 H. K. Manjili, H. Malvandi, M. S. Mousavi, E. Attari and H. Danafar, *Artif. Cells, Nanomed., Biotechnol.*, 2018, **46**, 926–936.
28 L. Wang, Y. Wang, X. Wang, L. Sun, Z. Zhou, J. Lu and Y. Zheng, *J. Microencapsulation*, 2016, **33**, 43–52.
29 C. Righeschi, M. Coronnello, A. Mastrantoni, B. Isacchi, M. C. Bergonzi, E. Mini and A. R. Bilia, *Colloids Surf., B*, 2014, **116**, 121–127.
30 P. Prabhu, S. Suryavanshi, S. Pathak, A. Patra, S. Sharma and V. Patravale, *Int. J. Pharm.*, 2016, **513**, 504–517.
31 S. Gurunathan, M.-H. Kang, M. Qasim and J.-H. Kim, *Int. J. Mol. Sci.*, 2018, **19**, 3264.
32 D. D. Lasic, *J. Colloid Interface Sci.*, 1990, **140**, 302–304.
33 S. S. Venkatraman, L. L. Ma, J. V. Natarajan and S. Chattopadhyay, *Front. Biosci., Scholar Ed.*, 2010, **2**, 801–814.
34 S. Vrignaud, J. P. Benoit and P. Saulnier, *Biomaterials*, 2011, **32**, 8593–8604.
35 S. Kalita, B. Devi, R. Kandimalla, K. K. Sharma, A. Sharma, K. Kalita, A. C. Kataki and J. Kotoky, *Int. J. Nanomed.*, 2015, **10**, 2971–2984.
36 S. Kaddah, N. Khreich, F. Kaddah, C. Charcosset and H. Greige-Gerges, *Food Chem. Toxicol.*, 2018, **113**, 40–48.
37 J. Shang and X. Gao, *Chem. Soc. Rev.*, 2014, **43**, 7267–7278.
38 M. V. Shaikh, M. Kala and M. Nivsarkar, *Eur. J. Pharm. Sci.*, 2017, **100**, 262–272.
39 C. Lambros and J. P. Vanderberg, *J. Parasitol.*, 1979, **65**, 418–420.
40 M. Smilkstein, N. Sriwilaijaroen, J. X. Kelly, P. Wilairat and M. Riscoe, *Antimicrob. Agents Chemother.*, 2004, **48**, 1803–1806.
41 W. Peters, J. H. Portus and B. L. Robinson, *Ann. Trop. Med. Parasitol.*, 1975, **69**, 155–171.
42 A. Budhian, S. J. Siegel and K. I. Winey, *Int. J. Pharm.*, 2007, **336**, 367–375.
43 WHO, *Guidelines for the treatment of malaria*, 3rd edition, 2015, http://apps.who.int/iris/bitstream/10665/162441/1/9789241549127_eng.pdf?ua=1, accessed April 28, 2020.
44 C. R. Alving, *Biochim. Biophys. Acta*, 1992, **1113**, 307–322.
45 J. Szebeni, L. Baranyi, S. Savay, J. Milosevits, R. Bunger, P. Laverman, J. M. Metselaar, G. Storm, A. Chanan-Khan, L. Liebes, F. M. Muggia, R. Cohen, Y. Barenholz and C. R. Alving, *J. Liposome Res.*, 2002, **12**, 165–172.
46 M. A. Dobrovolskaia, P. Aggarwal, J. B. Hall and S. E. McNeil, *Mol. Pharmaceutics*, 2008, **5**, 487–495.
47 J. Szebeni and S. M. Moghimi, *J. Liposome Res.*, 2009, **19**, 85–90.
48 J. Krücken, L. I. Mehnert, M. A. Dkhil, M. El-Khadragy, W. P. M. Benten, H. Mossmann and F. Wunderlich, *Infect. Immun.*, 2005, **73**, 6390–6398.
49 J. Szebeni, *Toxicology*, 2005, **216**, 106–121.
50 J. Szebeni, P. Bedocs, Z. Rozsnyay, Z. Weiszhár, R. Urbanics, L. Rosivall, R. Cohen, O. Garbuzenko, G. Báthori, M. Tóth, R. Bünger and Y. Barenholz, *Nanomedicine*, 2012, **8**, 176–184.
51 M. Mohamed, A. S. Abu Lila, T. Shimizu, E. Alaaeldin, A. Hussein, H. A. Sarhan, J. Szebeni and T. Ishida, *Sci. Technol. Adv. Mater.*, 2019, **20**, 710–724.
52 M. T. Cahill, B. T. Smith and S. Fekrat, *Am. J. Ophthalmol.*, 2002, **134**, 281–282.
53 N. M. La-Beck, X. Liu and L. M. Wood, *Front. Pharmacol.*, 2019, **10**, 220.
54 R. Gilabert-Oriol, G. M. Ryan, A. W. Y. Leung, N. S. Firmino, K. L. Bennewith and M. B. Bally, *Int. J. Mol. Sci.*, 2018, **19**, 2922.

55 P. Aggarwal, J. B. Hall, C. B. McLeland, M. A. Dobrovolskaia and S. E. McNeil, *Adv. Drug Delivery Rev.*, 2009, **61**, 428–437.
56 T. Efferth and B. Kaina, *Crit. Rev. Toxicol.*, 2010, **40**, 405–421.
57 R. Li, X. Li, L. Xie, D. Ding, Y. Hu, X. Qian, L. Yu, Y. Ding, X. Jiang and B. Liu, *Int. J. Pharm.*, 2009, **379**, 158–166.
58 J. Yang, S. B. Park, H.-G. Yoon, Y. M. Huh and S. Haam, *Int. J. Pharm.*, 2006, **324**, 185–190.
59 A. D. Sezer, J. Akbuğa and A. L. Baş, *Drug Delivery*, 2007, **14**, 47–53.
60 R. Muzzalupo, L. Pérez, A. Pinazo and L. Tavano, *Int. J. Pharm.*, 2017, **529**, 245–252.
61 A.-M. Fernández-Romero, F. Maestrelli, P. A. Mura, A. M. Rabasco and M. L. González-Rodríguez, *Pharmaceutics*, 2018, **10**, 256.
62 S. U. Rawal and M. M. Patel, in *Chapter 2, Lipid Nanocarriers for Drug Targeting*, ed. A. M. Grumezescu, William Andrew Publishing, 2018, pp. 49–138, DOI: 10.1016/B978-0-12-813687-4.00002-5.
63 A. F. Slater, *Pharmacology & Therapeutics*, 1993, **57**, 203–235.
64 Y. Yuthavong, B. Tarnchompoo, T. Vilaivan, P. Chitnumsub, S. Kamchonwongpaisan, S. A. Charman, D. N. McLennan, K. L. White, L. Vivas, E. Bongard, C. Thongphanchang, S. Taweechai, J. Vanichtanankul, R. Rattanajak, U. Arwon, P. Fantauzzi, J. Yuvaniyama, W. N. Charman and D. Matthews, *Proc. Natl. Acad. Sci. U. S. A.*, 2012, **109**, 16823–16828.
65 H. M. Ismail, V. Barton, M. Phanchana, S. Charoensutthivarakul, M. H. L. Wong, J. Hemingway, G. A. Biagini, P. M. O'Neill and S. A. Ward, *Proc. Natl. Acad. Sci. U. S. A.*, 2016, **113**, 2080–2085.
66 J. L. Bridgford, S. C. Xie, S. A. Cobbold, C. F. A. Pasaje, S. Herrmann, T. Yang, D. L. Gillett, L. R. Dick, S. A. Ralph, C. Dogovski, N. J. Spillman and L. Tilley, *Nat. Commun.*, 2018, **9**, 3801.